J. Synchrotron Rad. (1996). **3**, 1–5

A Novel Technique for Accurate Intensity Calibration of Area X-ray Detectors at Almost Arbitrary Energy

J. P. Moy,[a] A. P. Hammersley,[a] S. O. Svensson,[a] A. Thompson,[b] K. Brown,[b] L. Claustre,[b] A. Gonzalez[a] and S. McSweeney[b]

[a]*European Synchrotron Radiation Facility, BP 220, 38043 Grenoble, France, and* [b]*European Molecular Biology Laboratory, 38042 Grenoble, France*

(*Received 13 June 1995; accepted 3 October 1995*)

A novel intensity uniformity calibration method for area X-ray detectors is described. In diffraction experiments, amorphous lithium glass plates, containing doping elements chosen for their K edges just below the energy of the main beam, replace the crystallographic samples for the calibration measurement. The fluorescent emission excited by the X-ray beam is almost isotropic. It has exactly the same geometry as the diffracted radiation, and can be obtained at the same wavelength by proper selection of the element and excitation energy. A simple 2θ scan allows the emission distribution as a function of angle to be characterized with an accuracy of a fraction of a percent. This allows a flat-field correction to a similar accuracy. The quality of crystallographic data collected with an X-ray image intensifier/CCD detector was significantly improved by flat-field correction using an Sr-doped lithium tetraborate glass. This technique can be applied to X-ray energies from 5 to 50 keV; the calibration sample is small, stable and easily handled.

Keywords: X-ray detectors; detector calibration; uniformity; energy-dependent response.

1. Introduction

Accurate intensity calibration is a critical issue for all imaging X-ray detectors, including film, imaging plate, multiwire proportional chambers and CCD-based detectors. Molecular structure determination by diffraction is especially demanding as it implies accurate intensity measurements of Bragg reflections hitting the detector in different regions. In the case of anomalous dispersion, an accuracy of less than one percent is highly desirable (Thomas, 1990; Stanton, Phillips, Li & Kalata, 1992; Tate *et al.*, 1995).

A very promising modular detector system based on X-ray image intensifiers (XRII) and high-performance CCD cameras has been developed at the ESRF (Moy, 1994). It delivers images with more than a million pixels over a 220 mm diameter, and a dynamic range of 50 000:1 with a readout time of a few seconds, or 5000:1 with a readout time of less than 0.1 s. Detection quantum efficiency exceeds 30% from 5 to >50 keV.

A weakness of this system is the strong radial variation of intensity response. Consequently, non-uniformity corrections are of paramount importance. More generally, all area detectors exhibit some non-uniformity of response, either for low spatial frequencies, *e.g.* loss of sensitivity in the edges, variation of the thickness of the absorbing medium, or for high spatial frequencies, *e.g.* grain structure of the absorbing medium, pixel-to-pixel gain variations.

2. Uniformity of intensity response calibration techniques

A flat-field correction based on a uniform illumination, from an isotropic point source, or at least a well known distribution of X-rays, is the most practical way to take all these sources of non-uniformity into account. We will refer to an illumination which is close, but not totally uniform or isotropic, as a flood-field. Flood-field images should ideally be taken with a calibration source at the same energy and position as the diffracting sample, in order to reproduce effects connected with energy and incidence angle. The ideal point source should be monochromatic, isotropic, and should be available for the required energy, usually between 5 and 50 keV (Stanton *et al.*, 1992; Hammersley *et al.*, 1995). As long as an ideal isotropic point source is not available, it is necessary to characterize the intensity emission as a function of the position on the detector and correct the flood-field source emission for the distribution. For this correction process to introduce as little error as possible, it is important that the intensity distribution is as smooth and as close to isotropic as possible. Other two-dimensional detectors have been used to characterize such emissions, *e.g.* X-ray film (Stanton *et al.*, 1992). However, we believe that the best results may be obtained from a 2θ scan of a source which is axially symmetric about the X-ray beam with an appropriate detector.

Different methods to achieve this flood-field illumination have been used with varying degrees of success:

(*a*) *Elastic scattering* of the X-ray beam used for the diffraction experiment by an amorphous sample provides a monochromatic source at the same energy. Unfortunately, scattering is very far from isotropic (polarization and 2θ angle dependence) and is a very weak effect, so that even with a powerful beam it is quite difficult to obtain data over the whole sensitive area of the detector with good statistics.

(*b*) Following several authors (Stanton *et al.*, 1992; Strauss *et al.*, 1990), we have also used *radioactive sources* such as ^{55}Fe, ^{109}Cd or ^{241}Am. Their emission is not fully isotropic because of source imperfections such as the window shape, self absorption, and irregular distribution of the isotope. Revolving the source during exposure improves the situation, but this method remains unsatisfactory for a number of reasons:

(i) It takes a long time (hours or even days) to reach acceptable statistics on the detector, and the activity of the source results from a trade-off between the desired X-ray flux and realistic safety considerations. Such long exposures result in the build up of noise in some detectors.

(ii) The choice of energy is very limited, and except for ^{55}Fe at 5.9/6.4 keV, these sources are far from monochromatic.

(*c*) *X-ray fluorescence* is a good alternative as it should make it possible to achieve emission at almost any energy by selecting the appropriate element, and the fluorescent sample can easily be put in the same place as the diffracting sample (Thomas, 1990). The main difficulty with this method is obtaining an amorphous fluorescent sample to avoid Bragg reflections resulting in intense spots or rings that would spoil the flood-field pattern. A liquid solution is a good response to these requirements and this technique has been used (Otwinowski, 1994). However, we have met some practical limitations: the container needs windows which are often more structured than the liquid, so that some ring patterns appear on the flood image. It is also quite difficult to achieve the good parallelism of the faces necessary to ensure axial symmetry of the fluorescence and to make a leakproof cell small enough to be placed on the diffractometer head in the sample position. Using this technique, the authors could not get less than ~3% deviation from axial symmetry. A solid sample would obviously alleviate these problems. We tested several optical glasses containing heavy metals, but all had residual order resulting in a ring pattern. Amorphous metal alloys have been used (Thomas, 1990; Tucker, 1995) but they are limited to a few transition metals (Fe, Ni, Co, Mo) mixed in fixed proportions.

We recognized the great interest in X-ray fluorescence analysis as a potential source of amorphous fluorescent samples. The requirements for this technique are quite similar to our demands, insofar as diffraction spots or rings from the sample that might saturate the detector are prohibited. Therefore, a solid solution of the sample to be analysed in an amorphous lithium borate glass disc is often used. These glass discs can be made with almost any doping element, allowing an extremely wide range of fluorescence energies, in a weight concentration of up to 10%. These samples are chemically stable, easily handled, and can be thinned down to reach the optimal thickness at which the excitation beam is strongly absorbed whereas fluorescence is mainly transmitted. This is essential to ensure a high ratio of fluorescence to scattering which permits the 2θ scan correction. The relatively high weight concentration results in a typical thickness of less than one millimetre. These glass discs can also be very small, which allows them to be mounted in place of the sample.

3. Experimental setup

We have applied the latter technique to the correction of data acquired with the XRII/CCD detector. This test experiment was performed with a monochromatic 16.6 keV X-ray beam delivered by the D5 beamline of the ESRF, collimated down to 600 μm diameter. Test crystals were placed on the diffractometer head. We used a glass disc containing 10% of Sr (*K* edge at 16.1 keV, emission line at 14.2 keV) kindly provided by Philips Analytical. The slight difference in energy between data collection and calibration is not detrimental to its quality as both the Be windows and the CsI:Na scintillator of the XRII have their absorption edges very far from 14 keV. If necessary, the experiment could be carried out at the same energy as the calibration.

As regards fluorescence yield, the optimal mass per unit area, m, is assumed to be reached when the product (absorption at the excitation energy) × (transmission at the fluorescent energy) is maximum for normal incidence and emission. m is easily calculated:

$$m = \rho/\mu_{\rm exc} \ln[(\mu_{\rm exc} + \mu_{\rm fluo})/\mu_{\rm fluo}],$$

where $\mu_{\rm exc}$ is the absorption coefficient at the excitation energy and $\mu_{\rm fluo}$ is the absorption coefficient at the fluorescence energy.

For Sr, $\mu_{\rm exc}/\rho = 115\ {\rm cm^2\ g^{-1}}$ and $\mu_{\rm fluo}/\rho = 15\ {\rm cm^2\ g^{-1}}$. The best value is $m = 19\ {\rm mg\ cm^{-2}}$ of Sr, corresponding to a thickness of ~300 μm of a $5.7\ {\rm g\ cm^{-3}}$ $Li_2B_4O_7$ glass containing 10% of Sr. 99% of the excitation beam is absorbed, whilst 75% of the fluorescence is transmitted.

The glass disc is easily aligned orthogonal to the X-ray beam using the specular reflection of a laser beam shone through the collimator, or using an optical microscope as for sample alignment. This is quite important for obtaining good axial symmetry. We have made such glass samples with many elements, from Sc (4.09 keV) to Ta (57.5 keV), by melting $Li_2B_4O_7$ and the desired element oxide or carbonate in a platinum crucible (Foust, 1995).

The XRII is a 220 mm diameter active-area model 49425 HX from Thomson Tubes Electroniques. It has a Be window to extend its sensitivity down to ~5 keV. Its output phosphor screen is optically relayed onto the CCD by high-quality lenses. A mu-metal shield prevents magnetic influences and ensures image stability. The CCD cameras are slow scan, thermoelectrically cooled AT200 from Photometrics, using a Tektronix 1024^2 CCD with 24 μm square pixels and TE 1242E from Princeton Instruments with an EEV 1152 × 1242 pixels $22.5\ \mu{\rm m}^2$. The dynamic range is 16 000:1 (14-bit encoder) at a readout speed of 200 kpel s^{-1} (Photometrics) and 30 000:1 at 150 kpel s^{-1} for the Princeton Instruments system. The overall gain

of the system is adjusted by stopping down the lens to ~3 electrons in the CCD per detected X-ray quantum of 16 keV.

4. Results

Fig. 1 shows a folded 2θ scan of the emission of the Sr glass obtained with an Amptek photodiode counter; the main beam is blocked by a beamstop. The non-uniformity does not exceed $\pm 4\%$ from 0 to 30°. Furthermore, the ripples on the angular emission are symmetric within $\pm 0.5\%$ as shown by the excellent superposition of the points from both sides, and can easily be accounted for in the correction process.

The same plot shows the emission from a dysprosium sample. Its fluorescence energy is 46 keV, and the excitation energy is 54 keV (K edge at 53.8 keV).

The emission of the high-energy sample is not as smooth as that of the Sr sample. This is easily explained by several reasons:

(i) The variation in absorption coefficient across the K edge decreases with the atomic number (μ/ρ jumping from 15.7 to 115 $cm^2\ g^{-1}$ for Sr, and from 3.2 to 16.4 $cm^2\ g^{-1}$ for Dy). It is therefore all the more difficult to maintain a strong absorption of the excitation beam and a good transmission of the fluorescence as the Z number is increased. Diffraction rings become apparent on top of fluorescence, and oblique fluorescence is noticeably absorbed.

(ii) At high energies, the Compton shift becomes significant. For $2\theta = 30°$, $\Delta E = 51$ eV at 14 keV, and 520 eV at 45 keV. If the excitation energy is chosen too close to the K edge, Compton scattering above a given angle may fall below the edge and hence be transmitted. The main beam energy should be chosen to avoid this artefact.

Fig. 2 displays a flood-field image from the XRII/CCD detector illuminated by an Sr-doped glass sample, corrected for distortion and 2θ scan. The exposure time was 30 min in order to fill the 14-bit dynamic range of the detector, using the unfocused beam from a bending magnet. The same measurement was repeated using an ESRF wiggler, in less than 30 s.

The drop in sensitivity from the centre to the edge is *ca* 40%, very similar to the predicted drop from the XRII (≃25%) combined with the slight vignetting of the tandem lens (≃5%) and losses due to the incidence angle. The lack of circular symmetry results from the XRII non-uniformity of response, mainly due to the photocathode. Further refinement can be obtained by using the flood image for low and medium spatial frequency corrections and a visible light image from the CCD alone to correct for pixel response non-uniformity. The same fluorescent sample is also used to illuminate an array of pinholes for spatial distortion corrections (Hammersley, Svensson & Thompson, 1994).

Fig. 3(*a*) shows the flood-field illumination of an imaging plate (300 mm diameter Mar Research system) under the same conditions. The whole pattern is very smooth, without any sharp features. Taking into account the $1/\cos^3\theta$ geometric variation observed for a point source illuminating a plane surface, it is in good agreement with the 2θ scan. Fig. 3(*b*) shows the flood-field illumination obtained under the same conditions, except for a main beam energy below the K edge of Sr. Only scattering is now collected, and the effect of polarization is obvious. Fig. 3(*c*) displays the deviation from axial symmetry in the flood-field image of Fig. 3(*a*), which measures the systematic error introduced by the simple 2θ scan correction. At its extremes, its average value is $\pm 1.5\%$, and the overall r.m.s. value is $<1\%$. The deviation from axial symmetry owing to polarization may be corrected by subtracting a scaled version of the below-edge flood-field from the above-edge image. The scale factor may be

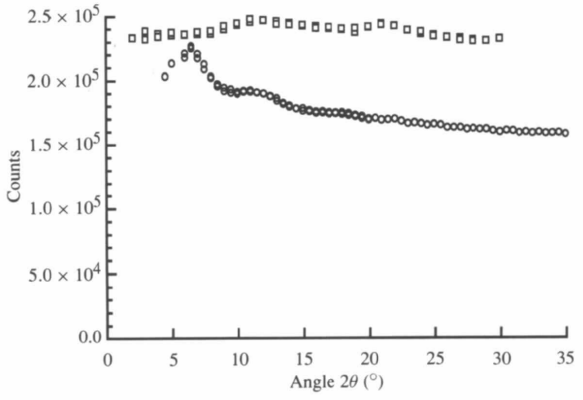

Figure 1
2θ scan of the fluorescence emission of an Sr-doped lithium tetraborate glass sample (squares) excited at 16.6 keV (fluorescence at 14.2 keV), and Dy-doped glass (circles) excited at 54 keV (fluorescence at 46 keV), measured with an Amptek photodiode counter.

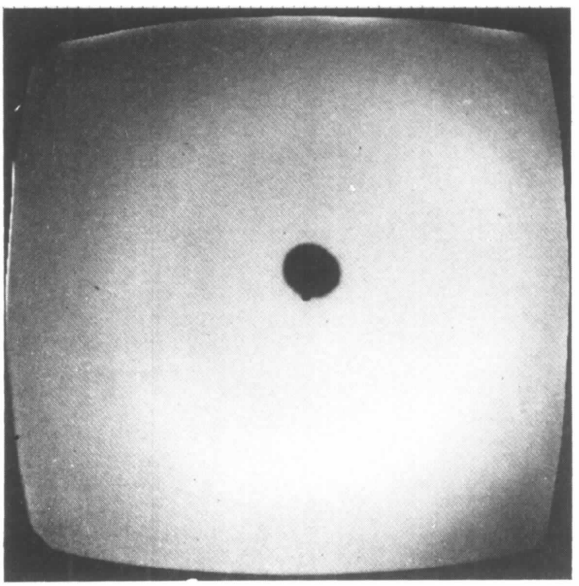

Figure 2
Emission of an Sr-doped glass sample recorded with the XRII/CCD detector (identical conditions to Fig. 1) after spatial distortion and the 2θ scan correction of Fig. 1 (Sr).

calculated from absorption coefficients for the transmitted elastic scattering at the two energies. The below-edge flood-field is corrected for the polarization effect and the same scaling factor applied. It is then added back to the above-edge image. This flood-field should be free of the effects of polarization and may be corrected to a flat-field image by dividing by a 2θ scan taken vertically (assuming 100% horizontal polarization). A much simpler alternative may be to use a thicker fluorescent sample. This will reduce the fluorescence yield, so that longer integration times will be necessary, but will more heavily attenuate the elastic scattering, so that the effect of polarization can be made insignificant. Fig. 3(*c*) also shows the effect of the Kapton strip used to support the beamstop, which is taken into

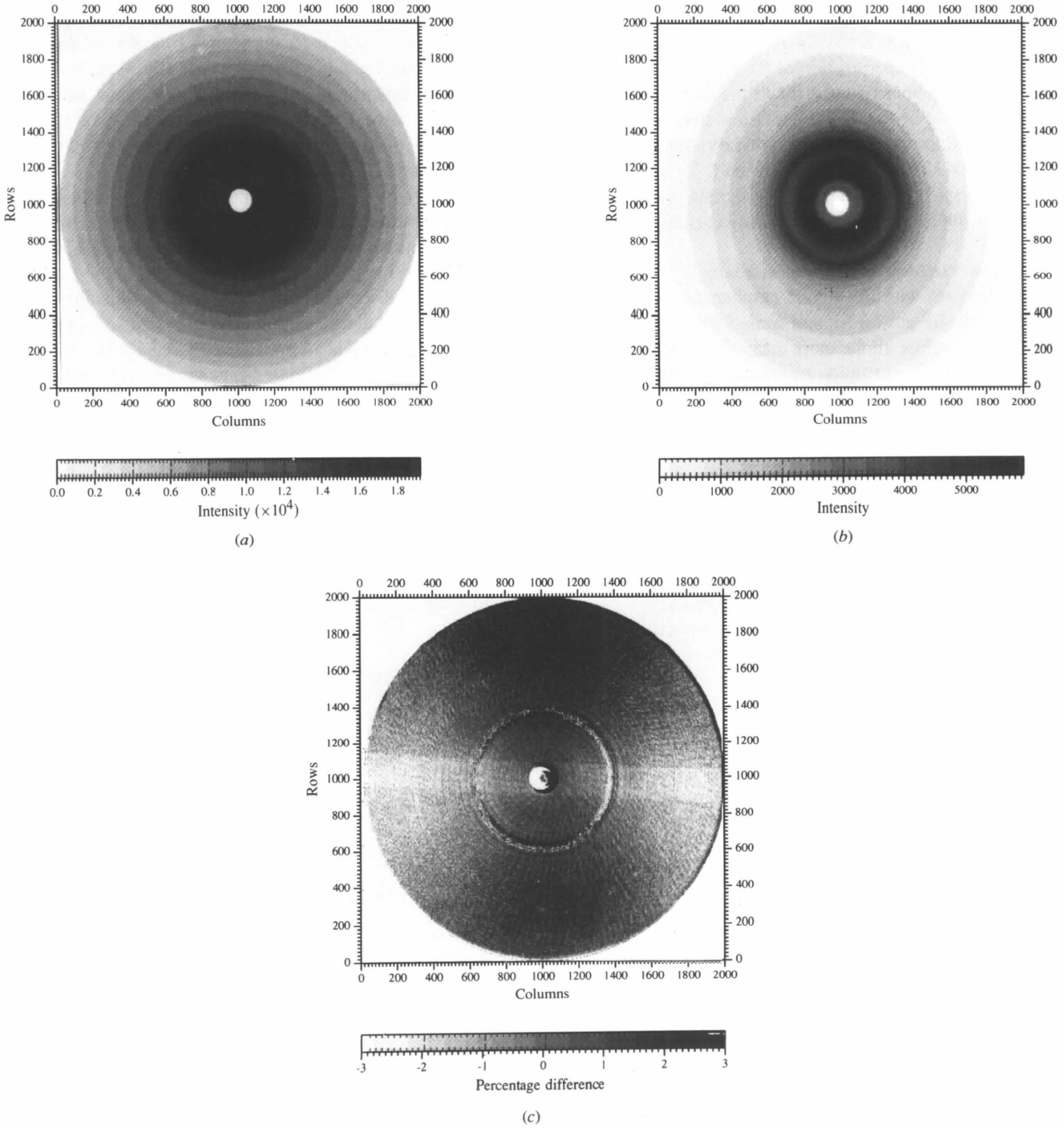

Figure 3
(*a*) Sr-doped glass sample emission recorded with a Mar Research imaging plate, at an excitation energy above the *K* edge of Sr, showing fluorescence and scattering. (*b*) As (*a*) but at an excitation energy below the *K* edge of Sr showing only scattering. (*c*) Deviation from axial symmetry of image (*a*).

account by the flat-field correction. The ring effect is an artefact caused by the 'gain switching' of the imaging plate scanner.

Test experiments using tetragonal hen egg white lysozyme (HEWL) crystals have been performed as part of the calibration tests of the XRII/CCD (Hammersley *et al.*, 1996). Data sets collected with flat-field calibration using the lithium borate glass on the ESRF Optics beamline in an unfocused monochromatic X-ray beam from a bending magnet source (see Fig. 4) show a distinct improvement in data quality compared with those calibrated with the fluorescence from a solution of strontium nitrate. Although the crystals used in the two experiments were from different crystallizations, they were similar in quality and size. The beam conditions (intensity, divergence, wavelength) on the beamline were also very similar, and no other change in the image correction procedure was used.

5. Conclusions

The use of doped lithium borate glasses is the best method we have discovered to obtain a smooth, almost isotropic illumination of a two-dimensional detector for flat-field correction. The calibration samples are solid state and are easily handled. They can be made with almost any element (only volatile elements or gases cannot be incorporated into the glass). Energies from a few keV to more than 50 keV can be reached.

Flat-field correction of data from the XRII/CCD detector makes it possible to collect diffraction data of a quality comparable with the best obtained with imaging plates but in a much shorter readout time: 5 s per image for this work. More generally, the improved flat-field correction made possible by this technique can significantly contribute to the accurate measurement of structure factors. Although this method was devised to meet the requirements of diffraction, it can obviously be adapted and used in a broader field of application.

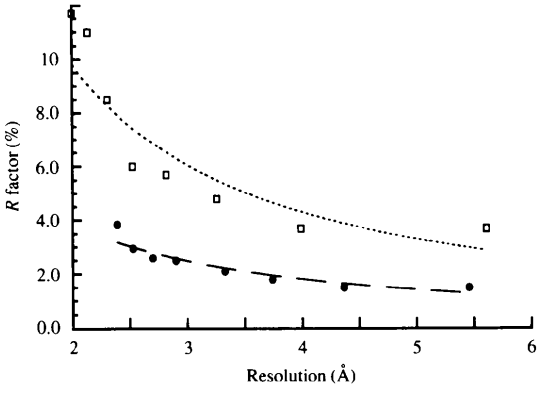

Figure 4
Comparison of the results obtained for HEWL with the two calibration methods: $Sr(NO_3)_2$ solution in a fluorescent cell (squares/dotted line) and Sr-doped glass (circles/dashed line). Note that all processing statistics are for fully and partially recorded reflections. Data were processed using *DENZO* (Otwinowski, 1993) and the *CCP*4 program suite (CCP4, 1979). Each frame was obtained in 180 s with a 1° oscillation.

We wish to thank F. Van Der Vlist from Philips Analytical for kindly providing the $Sr/Li_2B_4O_7$ glass disc as well as valuable advice, S. Foust who established the optimal conditions for making the glass samples during his training period, the ESRF Optics Group for their hospitality on the D5 beamline, H. Graafsma for the Dy sample measurement on ID11, and EMBL, Grenoble, for the loan of a Mar Research scanner.

References

CCP4 (1979). *A Suite of Programs for Protein Crystallography*, SERC Collaborative Computing Project No. 4. Daresbury Laboratory, Warrington, UK.
Foust, S. (1995). ESRF Internal Report (September 1995). ESRF, Grenoble, France.
Hammersley, A. P., Brown, K., Burmeister, W., Claustre, L., Gonzalez, A., McSweeney, S., Mitchell, E., Moy, J. P., Svensson, S. O. & Thompson, A. (1996). In preparation.
Hammersley, A. P., Svensson, S. O. & Thompson, A. (1994). *Nucl. Instrum. Methods*, A**346**, 312–321.
Hammersley, A. P., Svensson, S. O., Thompson, A., Graafsma, H., Kvick, Å. & Moy, J. P. (1995). *Rev. Sci. Instrum.* **66**(2), 1–5.
Moy, J. P. (1994). *Nucl. Instrum. Methods*, A**348**, 641–644.
Otwinowski, Z. (1993). *Data Collection and Processing*, edited by L. Sawyer, N. Isaacs & S. Bailey, pp. 56–62. SERC Daresbury Laboratory, Warrington, UK.
Otwinowski, Z. (1994). Private communication.
Stanton, M., Phillips, W. C., Li, Y. & Kalata, K. (1992). *J. Appl. Cryst.* **25**, 549–558.
Strauss, M. G., Westbrook, E. M., Naday, I., Coleman, T. A., Westbrook, M. L., Travis, D. J., Sweet, R. M., Pflugrath, J. W. & Stanton, M. (1990). *Nucl. Instrum. Methods*, A**297**, 275–295.
Tate, M. W., Eikenberry, E. F., Barna, S. L., Wall, M. E., Lowrance, J. L. & Gruner, S. M. (1995). *J. Appl. Cryst.* **28**, 196–205.
Thomas, D. J. (1990). *Proc. R. Soc. London Ser. A*, **428**, 181–214.
Tucker, P. (1995). Private communication.